

Article

Eco-Friendly Chitosan Composites: Transforming Miscanthus, Mushroom, Textile and Olive Waste into Sustainable Materials

Yasmina Khalaf ^{1,2} , Peter El Hage ^{1,3}, Souha Mansour ¹ , Nicolas Brosse ³ , Julia Dimitrova Mihajlova ², Anne Bergeret ⁴, Patrick Lacroix ⁵ and Roland El Hage ^{1,4,*} 

¹ Laboratory of Physical Chemistry of Materials (LCPM), Campus Fanar, Faculty of Sciences II, Lebanese University, Fanar, Jdeidet P.O. Box 90656, Lebanon; nina_khalaf@hotmail.com (Y.K.); hajjpeter9@gmail.com (P.E.H.); souha-mansour2010@hotmail.com (S.M.)

² Department of Mechanical Wood Technology, Faculty of Forest Industry, University of Forestry, 1756 Sofia, Bulgaria

³ Laboratoire d' Etude et de Recherche sur le Materiau Bois (LERMAB), Faculty of Science and Technology, University of Lorraine, Aiguillettes Boulevard, 54500 Vandœuvre-lès-Nancy, France; nicolas.brosse@univ-lorraine.fr

⁴ Polymers Composites and Hybrids (PCH), IMT Mines Ales, 6 Avenue de Clavières, 30100 Ales, France; anne.bergeret@mines-ales.fr

⁵ Greenpile, 18 Boulevard Edouard Lachaud, 19100 Brive La Gaillarde, France; greenpile-px@sfr.fr

* Correspondence: roland.el-hage@mines-ales.fr

Abstract: Recycling olive waste, a major by-product of the olive oil industry, presents significant environmental and economic benefits. This study explores the potential of olive waste (OW) by-products, specifically their individual components such as olive stones (OS), olive oily pomace (OS) and olive oil-free pomace (OF), as sustainable alternatives to wood in eco-friendly composite materials, alongside other residues such as miscanthus, spent mushroom substrate and recycled textile waste. Composite panels were produced with densities ranging from 685 to 907 kg/m³ through thermocompression. The manuscript details the production methodology and assesses the panel's thermal performance, water absorption, and mechanical strength. The aim is to assess the viability of these alternative materials in producing composites that could serve as environmentally friendly substitutes for traditional wood-based products. Oil-free pomace is a promising and effective alternative to wood, suitable for dry environments. Composite panels composed of miscanthus or spent mushroom substrate and oil-free pomace met the EN 312 standards for general-purpose products in dry conditions, highlighting their potential for use in sustainable applications.

Keywords: chitosan; agricultural and textile wastes; sustainable materials; mechanical properties; durability



Citation: Khalaf, Y.; El Hage, P.; Mansour, S.; Brosse, N.; Mihajlova, J.D.; Bergeret, A.; Lacroix, P.; El Hage, R. Eco-Friendly Chitosan Composites: Transforming Miscanthus, Mushroom, Textile and Olive Waste into Sustainable Materials. *AppliedChem* **2024**, *4*, 302–319. <https://doi.org/10.3390/appliedchem4030019>

Academic Editor: Jason Love

Received: 13 August 2024

Revised: 5 September 2024

Accepted: 11 September 2024

Published: 23 September 2024



Copyright: © 2024 by the authors. Licensee MDPI, Basel, Switzerland. This article is an open access article distributed under the terms and conditions of the Creative Commons Attribution (CC BY) license (<https://creativecommons.org/licenses/by/4.0/>).

1. Introduction

According to the United Nations, the Earth has lost more than 10 million hectares of forest per year over the past seven years due to deforestation. The increasing demand for wood products (lumber, logs, sawdust and wood chips) is one of the main causes [1]. Deforestation is a major environmental problem that contributes to climate change and threatens biodiversity. As a result, it becomes urgent to substitute wood with other ecofriendly raw materials in all wood-based products, especially the wood-based composites (WBP). Many agricultural residues and wastes that are poorly valorized, can constitute competitive, sustainable and environmentally friendly raw materials in the conception of WBP. Olive waste (OW) is a lignocellulosic residue from olive oil production, and constitutes a significant waste generated by this agro-industry. OW is reported as an environmental hazard that needs to be addressed due to its high phenolic content and the large amount of it that is produced in a short period of time. The production of virgin olive oil is showing global growth, and the increase in the quantities of this by-product requires us to consider new sustainable technologies of valorization [2]. A review of the literature shows that

different methods of the valorization of OW have been proposed, including the production of biomethane and bioethanol, use in heavy metal adsorbents, livestock feed, and use as a thermal insulation additive, in fertilizer or as a flame-retardant filler in polymers [2–5]. To the best of our knowledge, OW and its combination with other agricultural residues has never been used in the conception of wood-based composites.

Spent mushroom substrate (SMS) is a co-product generated during mushroom cultivation. It consists of lignocellulosic growth material (sawdust, sugarcane bagasse, wheat straw) and chitin-rich mushroom mycelium. Thus, SMS is not purely a physical material but contains significant organic matter as well. Generally, 5 kg of SMS is generated from the production of 1 kg of mushrooms. An average mushroom farm discards about 24 tons of SMS each month; this volume is increasing annually as the mushroom industry is steadily growing. Different routes for using SMS have been assessed in the fields of animal feed, bio-fertilizers, energy production, wastewater treatment and bioremediation [6–11]. SMSs have also been successfully used for the development of formaldehyde-free high-performance panels [12–14].

Miscanthus Giganteus (M) is a non-edible perennial grass that constitutes another interesting resource to substitute wood in the design of WCP, due to its high biomass yield, rapid growth, and similar composition to that of wood [15,16]. Over the past decade, much research has been conducted to investigate the suitability of miscanthus for use in sustainable materials by incorporating it into biosourced matrices such as poly(butylene adipate-co-terephthalate) (PBAT), starch, casein and gelatin [17–19]. It has also been successfully used in our group to produce chitosan-based insulation composites [20,21].

Textile fibers are produced in large quantities, with global consumption exceeding 110 million tons per year. This high production rate leads to a growing amount of textile waste. Among the most widely produced textiles are cotton and polyester, with cotton being prominently used in products like METISSE® jeans. These textiles, due to their substantial production volumes and widespread use, are of particular interest in recycling efforts. There is increasing interest in recycling these materials to enhance sustainability and mitigate environmental impacts. The composite materials sector presents a promising opportunity for incorporating recycled cotton and polyester fibers, potentially reducing waste and promoting circular economy practices [20,22–25].

Chitosan is an abundant polysaccharide extracted from the chitin of the exoskeleton of crustaceans, such as shrimps, lobsters and crabs. It is a non-toxic polymer that is soluble in aqueous acids and is useful as an effective bio-based adhesive for WCP [20,21,26–28]. The sustainable production of such composite panels also requires the replacement of existing petroleum-based synthetic adhesive systems with alternative products, such as polymers obtained from biobased, environmentally friendly and renewable resources [29–31].

In the present study, chitosan was selected as a natural binder for the conception of novel wood-based composites using different parts of olive wastes (olive pomace, olive stones and oil-free pomace) separately with miscanthus, spent mushroom substrate or textile wastes to the end of deeply comparing the physical, thermal and mechanical behavior of these composite panels.

2. Materials and Methods

2.1. Materials

Miscanthus and Giganteus (M) was provided by EARL Ar Gorzenn (Ferme de la Roselière, Pont-Croix, France). The spent mushroom substrate (SMS) was retrieved from the “Gourmet Mushroom” farm (Byblos, Lebanon). SMS produced during two mushroom harvests, and consisting initially of wheat straw and oyster mushrooms, was spread out for a week on the laboratory benches after arrival to air dry them before usage. Recycled textile fibers (T) from jeans, namely, METISSE® with an average length/diameter of 6 ± 3 mm/ 15 ± 3 μ m, were provided by Le Relais Co. (Billy-Berclau, France) and were used as received. Olive waste (OW) was retrieved from the “Ghaoui-Ghaoui” olive oil mill (Darbechtar, Lebanon). This OW, resulting from oil extraction treatment by cold-pressing

based on crushing the olives using a rotating mill followed by filtration to separate oil, was cured in the open air for a week after receiving it before being utilized. A commercial chitosan powder with an average molecular weight of $250,000 \text{ g}\cdot\text{mol}^{-1}$, a viscosity of 30–100 cps and a deacetylation degree above 90% was purchased from Glentham Life Sciences (UK) and was used as an adhesive binder. Glacial acetic acid with a purity $\geq 99.7\%$, purchased from VWR International (Les Ulis, France), was used as received for chitosan dissolution. Pure toluene and pure dichloromethane purchased from Carlo Erba Reagents (Le Bourget, France) and ethanol with a purity of 96% and purchased from VWR Chemicals (Les Ulis, France) were used as received.

2.2. Reinforcements Preparation

Dried M and SMS of 8 wt. % relative humidity and an OW of 7 wt. % relative humidity were milled using a Moulinex® (Écully, France) coffee grinder. OW was then manually sieved using a 2 mm pore size sieve to separate the oily pomace (OP) from olive stones (OS), which was mechanically crushed in a cement plant prior to sieving it. All components, i.e., OS, OP, M and SMS, were sieved separately using a MATEST electromagnetic sieving machine (Treviolo (BG), Italy) to collect the particles retained by the filters with a porosity of 1.18 mm for OS and OP and a porosity of $850 \mu\text{m}$ for M and SMS, as used in this study. A portion of sieved OP was weighed properly, placed in a cellulose cartridge, and then washed in a toluene/ethanol mixture (2/1 *v/v*) then with ethanol alone using a Soxhlet extractor equipped with a cooler on the top. The solvent mixture was heated to reflux for 24 h to eliminate the remaining oil. The oil-free pomace (OF) was dumped onto a Teflon-coated metal plate and completely dried in the oven for 2 h at $105 \text{ }^\circ\text{C}$ prior to use. Photographs of the different reinforcements, as received and used, are shown in Figure 1.

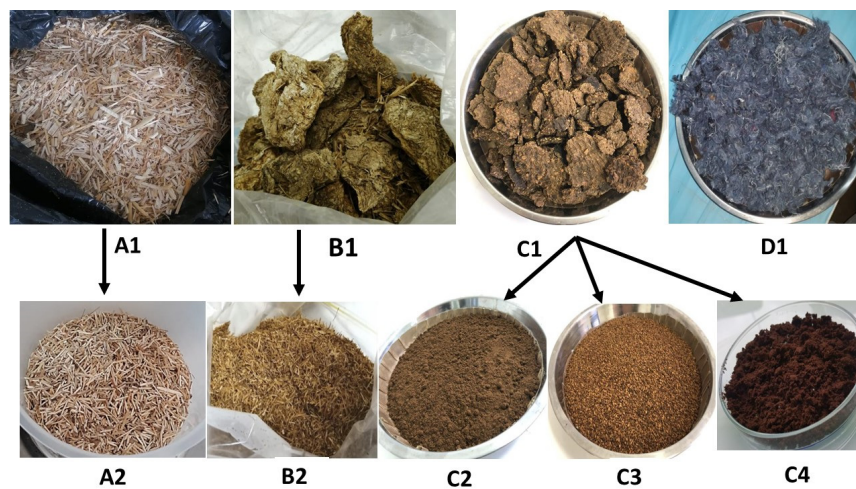


Figure 1. Selected reinforcements for the composite processing: (A1) M as received, (A2) M as used, (B1) SMS as received, (B2) SMS as used, (C1) OW, (C2) OP, (C3) OS, (C4) OF, (D1) T.

2.3. Composites Manufacturing

Nine formulations of composite panels were manufactured with different components, as summarized in Table 1. To prepare the 4% (*w/v*) chitosan binder solution, 4.5 g of chitosan powder was dissolved in 108 mL of 2% (*w/v*) glacial acetic acid solution at room temperature by mechanical stirring (1560 rpm) for 30 min until obtaining a homogeneous solution. Then, 24 g of OP, OS or OF, according to each formulation, was added to the binder solution and stirred again for 5 min to ensure a good dispersion of these particles in the solution. After that, the mixture was poured over 36 g of M, T or SMS followed by manual mixing before leaving it to stand for 30 min to ensure the good wettability of the reinforcements. Before molding, the mixture was preheated for 60 min at $105 \text{ }^\circ\text{C}$ to achieve a 30 wt. % relative humidity. Afterward, the pre-heated mixture was filled into a $180 \times 50 \times 70 \text{ mm}^3$ stainless steel mold coated with a self-adhesive backing Teflon sheet and compacted at room temperature to reach

a thickness of 1 cm, using a backing mold and a hydraulic press. The compacted mixture was then placed in an oven at 105 °C overnight (15 h) until totally dried while maintaining the compaction. Finally, the composite was removed from the mold and conditioned for 2 days in a climate-controlled room before testing.

Table 1. Compositions of the nine different formulations.

Formulation Labels	Types of Wastes (60/40 w/w)	Wastes Weight (g)	Dry Chitosan (g)	Ratio Wastes/Chitosan (wt. %)
MOP	Miscanthus/olive pomace	60	4.5	93/7
MOS	Miscanthus/olive stones	60	4.5	93/7
MOF	Miscanthus/oil-free pomace	60	4.5	93/7
SMSOP	Spent mushroom substrate/olive pomace	60	4.5	93/7
SMSOS	Spent mushroom substrate/Olive stones	60	4.5	93/7
SMSOF	Spent mushroom substrate/oil-free pomace	60	4.5	93/7
TOP	Textile wastes/olive pomace	60	4.5	93/7
TOS	Textile wastes/Olive stones	60	4.5	93/7
TOF	Textile wastes/oil-free pomace	60	4.5	93/7

2.4. Chemical Composition Analysis of Reinforcements Materials

Extractives contents were measured in 2 g of each reinforcement under reflux for 6 h using a Soxhlet apparatus with dichloromethane for SMS, M and OS and with toluene/ethanol mixture (2/1 v/v) for OP. They were calculated according to Equation (1),

$$\text{Extractivescontent(\%)} = 100 \cdot \frac{m_e}{m_i} \quad (1)$$

where m_e is the mass in g of dry extractive-free specimens and m_i is the mass in g of the initial native dry fibers.

Carbohydrate and Klason lignin contents were measured on extractive-free specimens.

Klason lignin was measured according to the laboratory analytical procedure (LAP) provided by the National Renewable Energy Laboratory (NREL). Here, 0.175 g of the specimen was hydrolyzed with 1.5 mL of 72% sulfuric acid in a water bath at 30 °C for 1 h, and then diluted with 42 mL of deionized water and autoclaved for 1 h at 120 °C before being filtered and dried for 2 h at 105 °C. The Klason lignin content was calculated according to Equation (2),

$$\text{Klason Lignin(\%)} = 100 \cdot \frac{m_L(\text{g})}{m_i(\text{g})} \quad (2)$$

where m_L is the mass of lignin recovered and m_i is the initial mass of fibers with extractives.

Monomer sugar contents in the liquid fraction obtained after filtrating and washing the specimen were quantified using high-performance anion-exchange chromatography with pulsed amperometric detection (HPAEC 6 PAD) (ICS-3000 Dionex, Dionex Corporation, Sunnyvale, CA, USA). All these measurements were performed three times for each specimen and the results are reported as a percentage of the original specimen.

2.5. Apparent, Bulk Density and Porosity Measurements

The calculated apparent density was obtained using the standard formula of the ratio of the mass and volume of each panel. The bulk (actual) density was measured on small cubes of each formulation using a density kit by measuring the mass (m) of a small cube in air and then in ethanol according to the following Equation (3):

$$\rho_{bulk} = \frac{m_a}{m_a - m_{eth.}} \cdot \rho_{eth.} \quad (3)$$

where m_a is the mass of the specimen measured in air, $m_{eth.}$ is the mass of the specimen measured in ethanol and $\rho_{eth.}$ is the density of ethanol.

The porosity rate ($\varepsilon(\%)$) is calculated using the following Equation (4), which considers the apparent ($\rho_{app.}$) and bulk densities (ρ_{bulk}) of each specimen:

$$\varepsilon(\%) = 100 \cdot \left(1 - \frac{\rho_{app.}}{\rho_{bulk}} \right) \quad (4)$$

2.6. Thermal Conductivity Properties

An FP2C conductimeter from NeoTIM (Neuilly-Plaisance, France), with a 50 mm planar thermal shock probe and linked to a computer for monitoring and signal processing, was used to measure the thermal conductivity (λ) of the panels. An energy source of 0.06 W, a thermal resistance of 12.5 Ω and a duration of 120 s were applied for each analysis.

Tests were conducted on three specimens of each formulation having $180 \times 50 \times 10 \text{ mm}^3$ dimensions at room temperature (20 °C).

2.7. Surface Contact Angle Property Measurements and Analysis

To evaluate the wettability of the panel's surfaces, Contact Angle Goniometer (Sheffield, UK) was used. The analysis set-up included a high-resolution USB camera and manual lens, powerful backlighting, and an adaptable specimen stage. The profiles of each drop of demineralized water deposited on the specimen's surface by a 1 μL pipette were recorded. Contact angle values were obtained by locally analyzing the profile of each drop based on the tangent method.

2.8. Water Absorption Capacity and Thickness Swelling by Immersion Properties

Water absorption capacity and thickness swelling were measured on panels of each formulation soaked in cold water. The mass and thickness of each panel were measured at different immersion times. At a specific time, specimens were removed from the water and wiped to remove excess water before each measurement. Immersion was stopped when saturation was reached in all the panels.

The water absorption capacity (%) was determined according to the following Equation (5):

$$\Delta m = 100 \cdot \left(\frac{m_t - m_0}{m_0} \right) \quad (5)$$

with m_t being the mass at a time t and m_0 the initial mass before immersion.

The thickness swelling, T_s (%), was determined according to the following Equation (6):

$$T_s = 100 \cdot \left(\frac{t_t - t_0}{t_0} \right) \quad (6)$$

with t_t being the thickness at time t and t_0 being the initial thickness before immersion.

2.9. Optical Microscope Observation

Surface observations of the panels were evaluated using a Ladybird MZ1240 Trinocular stereomicroscope (Neydens, France). Photographs were captured using a "MICROS CAM500" 5 MP CCD camera (The Woodlands, TX, USA) with a standard overall magnification of 100 \times . The observed images have been viewed and processed using the "MICRO-VISIBLE" program. These observations were made on $25 \times 15 \times 10 \text{ mm}^3$ specimens of each formulation before and after the immersion test.

2.10. Experimental Methods for Assessing Mechanical Properties

The compression test was performed on the Servo plus press (Castelfranco Veneto (TV), Italy) with a 1 ton load cell and cross head speed of 0.1 kN/s on specimens of each formulation before and after the water immersion test. Two specimens ($50 \times 50 \times 10 \text{ mm}^3$) of each formulation were compressed in the opposite direction of the panel's compaction, and one was compressed during its manufacturing to measure the compressive strength of each panel.

The three-point bending test was performed on three specimens of each formulation, according to NF EN 310, using an Instron 4206 universal testing machine (Norwood, MA, USA) equipped with a 100 kN capacity load cell at a speed of 5 mm/min at 20 °C. Force versus displacement graphs were constructed (example: Figure S1 in the Supplementary Material). The modulus of elasticity (MOE) and the bending strength (MOR) were determined on at least three specimens of each formulation with dimensions of $180 \times 50 \times 10 \text{ mm}^3$ according to Equation (7) and Equation (8), respectively.

$$MOE = \frac{l_1^3}{4bt^3} \cdot \left(\frac{F_2 - F_1}{a_2 - a_1} \right) \quad (7)$$

$$MOR = \frac{3F_{max} \cdot l_1}{2b \cdot t^2} \quad (8)$$

Here, l_1 is the distance between the support centers (120 mm in this study), b is the width of the specimen (in mm), t is the thickness of the specimen (in mm), F_{max} is the maximum (breaking) force (in N), $F_2 - F_1$ are the increase in force (in N), and $a_2 - a_1$ are the increase in displacement at the mid-length of the specimen (in mm).

The internal bond (IB) strength of each panel was assessed using a perpendicular tensile test according to the NF EN 319 with an Instron 4206 universal testing machine. At least three $50 \times 50 \times 10 \text{ mm}^3$ specimens of each formulation were analyzed with a 5 kN capacity load cell and a 2 mm/min pulling speed at 20 °C, and the IB was determined using Equation (9).

$$IB = \frac{F_{max}}{a \times b} \quad (9)$$

Here, F_{max} is the breaking stress (N), a is the length of the specimen (mm) and b is the width of the specimen (mm).

3. Results

3.1. Chemical Composition of Reinforcements

Table 2 shows the main compositions of the different reinforcements used in panel production. All the reinforcements used contain cellulose, hemicellulose, lignin and extractives in different proportions. M particles showed a very similar composition as wood, and the results obtained are in accordance with those of Sørensen et al. and El Hage et al. [24,32]. The richest reinforcement here was in cellulose (about 40% in weight), while it had the lowest extractives content (<1%). Conversely, OP showed the highest extractives content (about 26%), which was expected since OP contains residual phenolic compounds and fatty acids [33]. OS and OP showed similar cellulose, hemicellulose and lignin contents, but different extractives contents, as OS presented a low content (about 5%). SMS had the lowest hemicellulose content (about 10%). The lignin contents in all the reinforcements were almost the same (around 26%).

Table 2. Chemical compositions of reinforcements.

Reinforcement	Cellulose (%)	Hemicellulose (%)	Lignin (%)	Extractives (%)
OP	22.55 ± 1.59	21.6 ± 0.97	28.37 ± 0.26	26.28 ± 0.13
SMS	20.91 ± 0.21	9.99 ± 0.35	25.08 ± 0.96	5.06 ± 0.49
OS	22.92 ± 2.50	24.75 ± 2.06	26.03 ± 0.52	6.16 ± 0.13
M	40.07 ± 2.54	21.20 ± 1.40	26.72 ± 0.37	0.95 ± 0.01

3.2. Panels Apparent Density, Porosity and Thermal Conductivity

Photographs and the porosity rate variation as a function of the apparent density obtained for the prepared panels are presented in Figures 2a and 2b, respectively. It seems that the bulk density values varied greatly depending on the nature of the reinforcements used, between 685 ± 80 and $907 \pm 28 \text{ kg/m}^3$, with the densities of panels based on spent mushroom substrate (SMS) being much higher (806 ± 14 – $907 \pm 28 \text{ kg/m}^3$) compared to the others (665 ± 80 – $774 \pm 20 \text{ kg/m}^3$). This is related to the volume shrinkage of SMS-

containing specimens (Figure 2a), which can be explained by the collapse of the microtubes inside the cells and by the occurrence of adhesion phenomena in the mycelium, resulting in higher densities [12]. It is also clear that, with increasing bulk density, the porosity rate decreased, despite its low values. The most porous panels were TOP, MOS and SMSOS, with porosity rates of 22%, 19% and 16%, respectively, while the least porous were SMSOF (3%) and SMSOP (10%), which can be explained by the softening and shrinkage of the mycelium due to the high drying temperature (105 °C), inducing a decrease in the intrinsic porosity of the SMS [12]. The remaining panels showed an intermediate porosity. The results also show that when using OF instead of OP, the absence of extractives led to a denser, less porous and more compact panel.

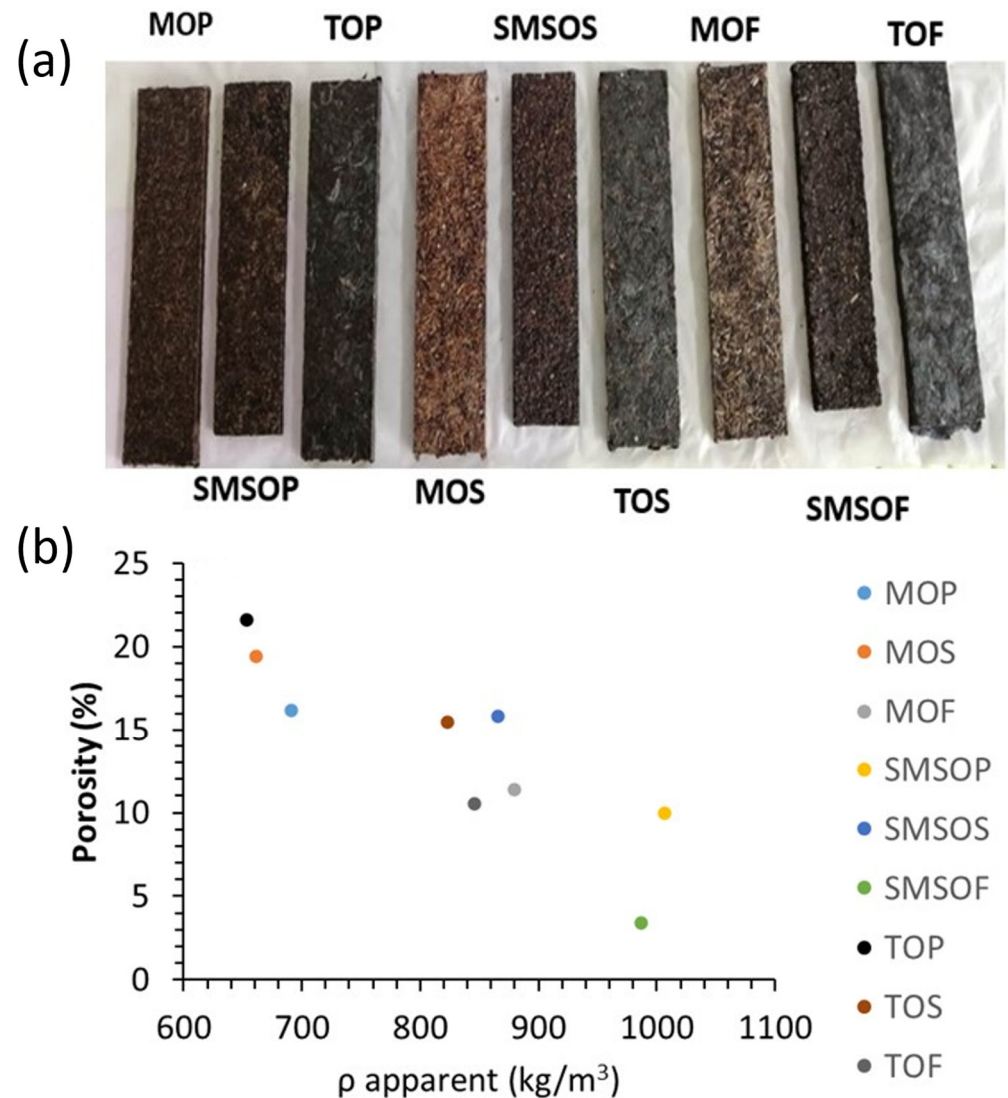


Figure 2. (a) Photographs of the different panels and (b) porosity variation as a function of apparent density of the panels.

The thermal conductivity values of the different panels are presented in Figure 3a. The thermal conductivity variation as a function of the density of the panels is presented in Figure 3b. A slight decrease in values can be observed with the decrease in density and increase in porosity. Therefore, with increases in porosity, the proportions of void spaces or air within the material increased. Air has significantly lower thermal conductivity compared to a solid material. Therefore, as the volume fraction of a solid decreases and the volume fraction of air increases, the overall thermal conductivity of the material decreases in a linear fashion. This observation agrees with those shown in the literature [20,34].

These high λ values could also be influenced by the presence of chitosan on the surfaces of the specimens, which is a conductive matrix with a conductivity of $0.32 \text{ W}\cdot\text{m}^{-1}\cdot\text{K}^{-1}$ [35].

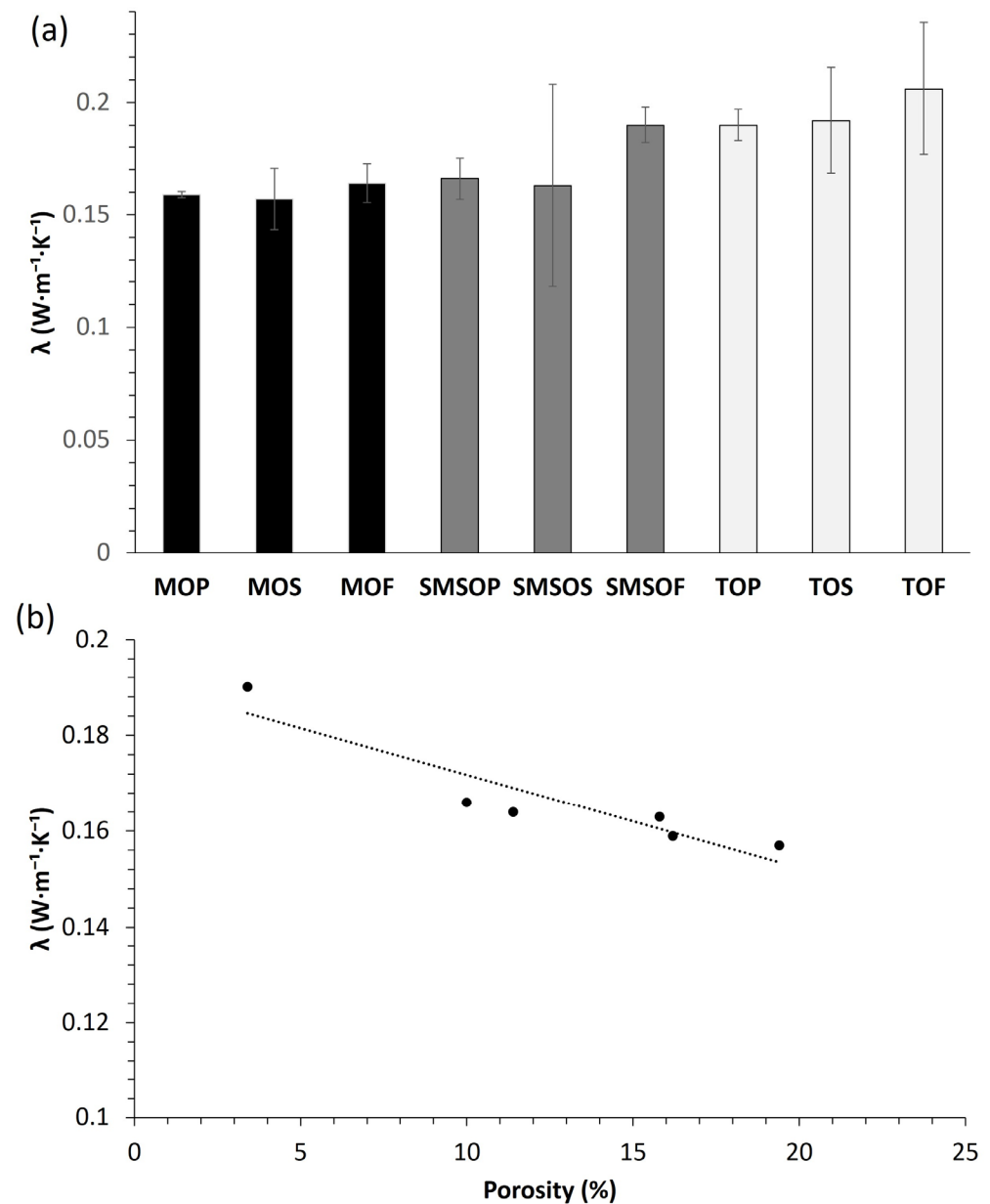


Figure 3. (a) Thermal conductivity of the panels; (b) thermal conductivity variation as a function of the density of the panels.

3.3. Optical Microscopic Observations

The dispersion and orientation of the reinforcements, the interfacial compatibility of the different constituents and the presence of voids are evaluated by microscopic observations. Figures 4a and 4b, respectively, show surface and cross-sectional observations of the different panels. The glossy layer observed on the surface of the particles corresponds to the presence of the chitosan binder. This indicates a good wetting of the various particles by the binder, which agrees with the results in the study of El Hage et al. [2].

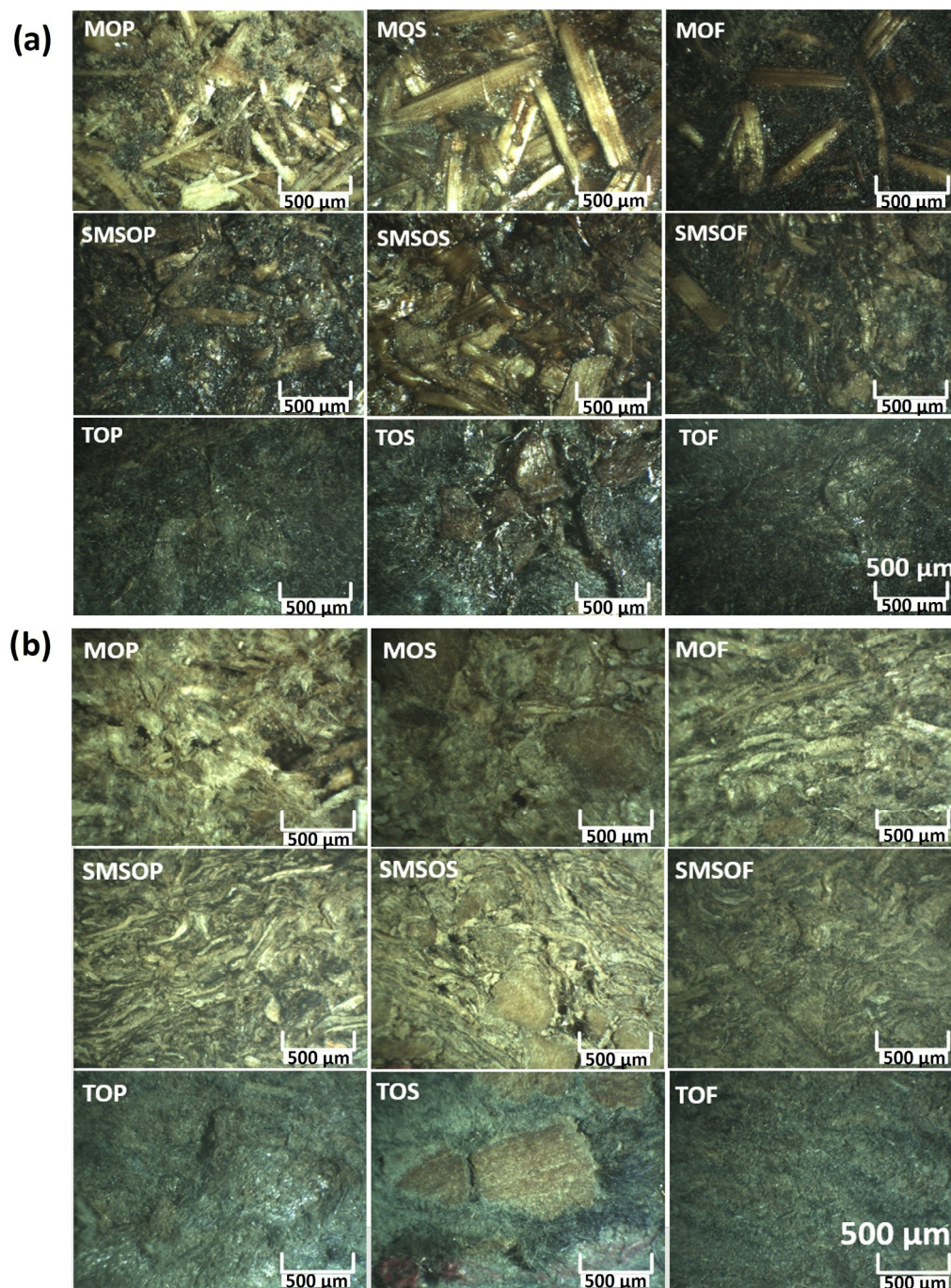


Figure 4. (a) Surfaces and (b) cross-sections of the different panels, with a scale of 500 μm applied to all figures.

It is clear that M, SMS and T were well dispersed, and were oriented homogeneously and parallel to the surface. It seems that OS was dispersed in the form of aggregates on the surface and was present in bulk on the different fibers (Figure 4a,b). Voids are clearly visible between the OS and the other fibers, indicating an interface problem. OF-based panels (MOF, TOF and SMSOF) do not show visible porosity, as observed in the presence of extractives in the OP-based panels (MOP, TOP and SMSOP). This indicates that the absence of extractives in the OF is related to the presence of large pores, which agrees with the results obtained previously (Figure 2).

3.4. Surface Contact Angle Properties

The surface wettability of the panels can be assessed by contact angle, which is the angle at the interface between water, air and a solid [36]. As shown in Figure 5, the OS-based panels (MOP = 114.82°, TOP = 118.89° and SMSOP = 111.57°) exhibited water-repellent behaviors, probably due to the presence of fatty acids (mainly oleic acid) [33]. On the other hand, the other panels produced from OS or OF presented hydrophilic behaviors.

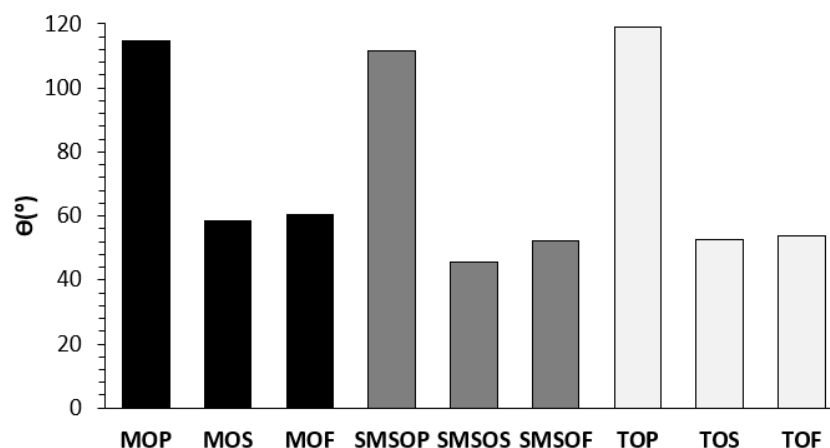


Figure 5. Contact angles of the different panels.

3.5. Water Absorption Capacity and Thickness Swelling

The panels were immersed in water to assess their durability and behavior in an aqueous environment. Figure 6 shows the water absorption capacity (Δm) of the panels during the first 30 min of immersion (Figure 6a) for the first 5 days (Figure 6b), and the thickness swelling (TS) during the 5 days. It seems that the absorption capacity of all composites is partially dependent on the nature of the olive wastes and the reinforcements used. Moreover, both the wettability characteristics of the different reinforcements and the nature of the interface seem to be major parameters that impact the absorption phenomenon's variation. For a short immersion period (30 min), the absorption capacities follow the following order: MOF < MOS < SMSOP < MOP < TOP = SMSOF < TOS < TOF < SMSOS. SMSOP and M-based panels showed a low absorption capacity ($\Delta m < 10$ wt. %), whereas SMSOS and TOF panels showed the highest absorption capacity ($\Delta m = 27$ –30 wt. %). With a long immersion time (5 days), MOP panels showed a significant gain in mass at saturation, and reached the threshold of 40 wt. %. This agrees with the microscopic observations, where voids and gaps between particles were observed for the MOP panel. In contrast, the SMSOF panel, which had a more compact structure, showed the lowest mass gain at saturation ($\Delta m \approx 30\%$). This behavior is caused by the absence of oil in the OF and the presence of mycelia in the SMS, which reacted by improving the interface between the various constituents [12].

Concerning the thickness swelling, it is clear from Figure 6c that after 5 days, TOF panels showed the highest TS (19%), which is probably linked to the hydrophilic nature of textile fibers and the absence of oil in the OF. Contrariwise, MOP panels showed the lowest TS (6%) but the highest mass gain, which can be explained by the double effect of the good wettability of reinforcements due to the chitosan and the presence of extractives in the OP forming a fixed structure, which absorbs water and maintains a good dimensional stability. The remaining panels showed intermediate TS values between 8% and 12%.

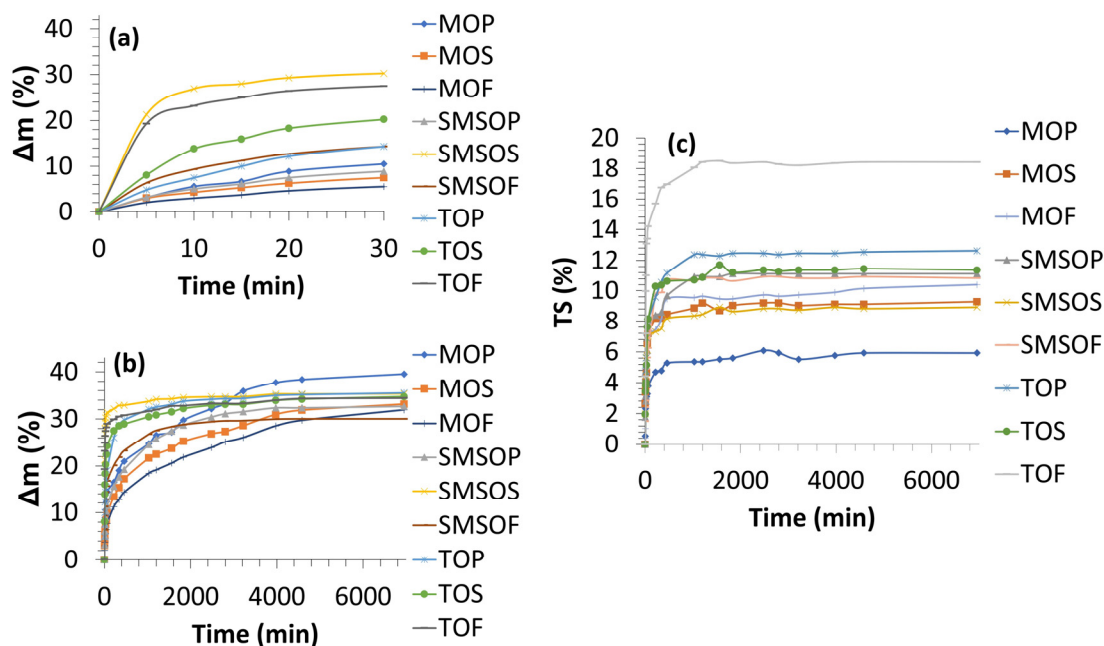


Figure 6. Water absorption capacity of the different panels (a) for 30 min; (b) for 6000 min; (c) thickness swelling of the different panels obtained by water immersion test.

3.6. Mechanical Properties

3.6.1. Bending Properties

Figure 7 shows modulus of elasticity (MOE, Figure 7A) and bending strength (MOR, Figure 7B) of the panels. The statistical analysis of the bending results, including the median value, the minimum, the maximum, the mean and the standard deviation of the MOE and the MOR, is shown in Table 3. It can be observed in Figure 7A that miscanthus-based panels (MOP, MOS and MOF) displayed the highest rigidity. Thus, the highest median MOE value was observed for MOS (1676 MPa) and the lowest for SMSOP (796 MPa). From the MOE values, it can also be noted that for all formulations, the presence of OF instead of OP improved the rigidity of the panels. This behavior can be linked to the better interface observed following microscopic observation (Figure 5) and to the more compact and less porous panels. It could be inferred from the bending strength values shown in Figure 7B that M-based panels also showed the highest MOR median, ranging from 6.3 MPa to 12.7 MPa, whereas SMS-based panels and T-based panels showed lower strength (2.3 to 5.2 MPa). Based on a previous study, this could be related to differences in the intrinsic mechanical properties of the fibers used, as we found that M-based panels showed better EOM and MOR values than T-based panels [21]. The same trend can be noted regarding the median MOR and MOE values for OF-based and OP-based panels, as the median bending strengths of MOF, SMSOF and TOF were greater than those of MOP, SMSOP and TOP, respectively. It is also clear that MOS showed the best bending properties between the OS-based panels. The median MOE and MOR values (1676 and 9.5 MPa) were, respectively, higher than those of SMSOS (1370 and 5.3 MPa) and TOS (1281 and 4.4 MPa). This behavior can be linked to the rigid and soft nature of OS and OP, respectively, but not to the porosity or the density of the specimens. When compared with some of the results from the literature, we can infer that the panels in our study showed lower MOE and MOR values than the panels made from sugarcane bagasse [37] and from sunflower stalks [38], whereas their MOE and MOR are similar to those of panels made from rice straw [39], kiwi pruning [40] and peanut hull [41]. The bending strength (MOR) value of the MOF panel (12.7 MPa) was sufficiently greater than the minimum requirements (10.5 MPa) set by the EN 312 standard [42] for particleboard panels intended for general purposes in the same thickness range (type P1).

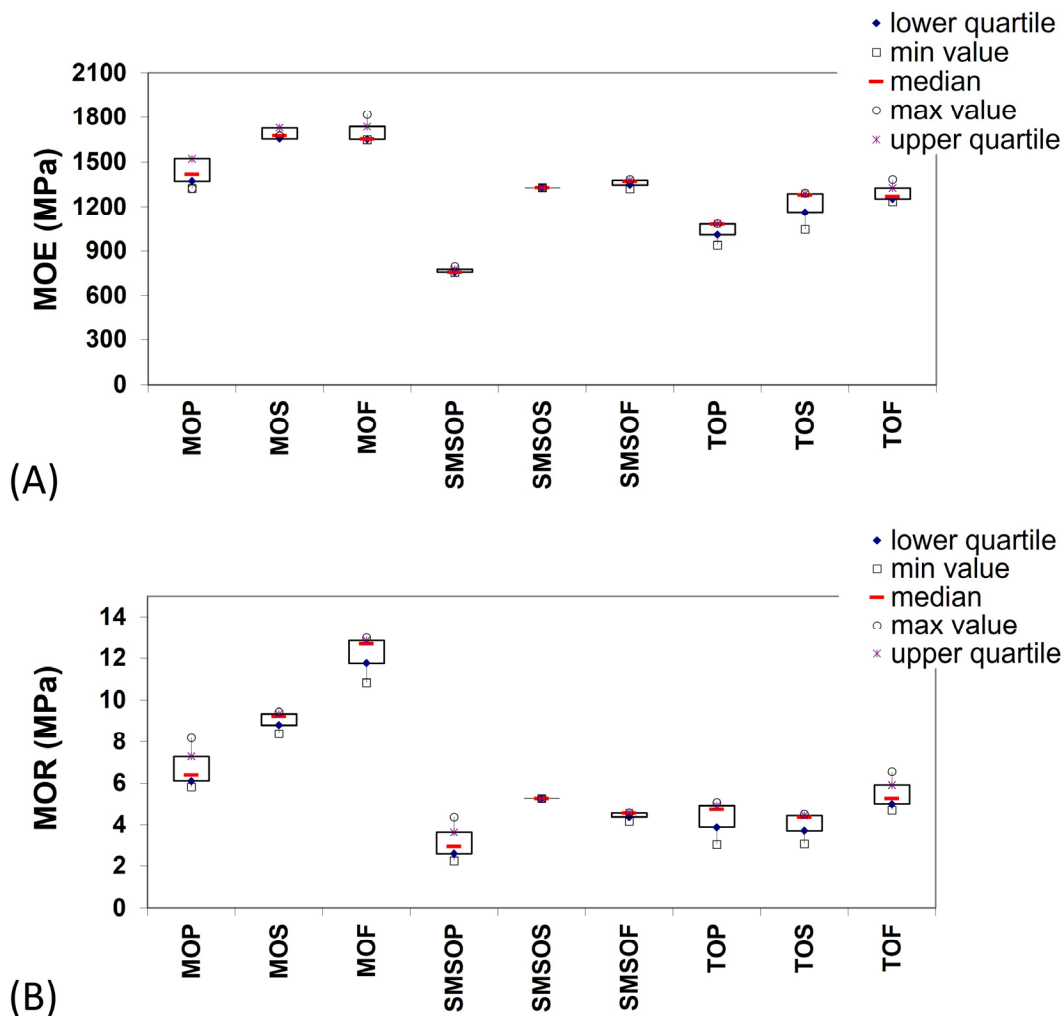


Figure 7. Bending properties of different panels: (A) modulus of elasticity (MPa); (B) bending strength (MPa).

Table 3. Statistical analysis of bending MOE and MOR results.

Formulations Labels		MOP	MOS	MOF	SMSOP	SMSOS	SMSOF	TOP	TOS	TOF
MOE values (MPa)	median value	1418.6	1676.0	1653.3	758.1	1328.7	1370.7	1079.7	1281.4	1270.0
	maximum value	1622.9	1779.2	1817.8	796.1	1328.7	1383.8	1085.1	1292.4	1382.7
	minimum value	1324.3	1632.9	1648.4	756.5	1328.7	1322.8	939.4	1045.8	1235.5
	mean value	1455.2 ± 152.6	1696 ± 75.2	1706.5 ± 96.4	770.2 ± 22.4	1313.7 ± 23.7	1359.1 ± 32.1	1034.7 ± 82.6	1206.5 ± 139.4	1296.1 ± 77
MOR values (MPa)	median value	6.4	9.2	12.7	2.9	5.3	4.6	4.8	4.4	5.3
	maximum value	8.2	9.5	13.0	4.4	5.3	4.6	5.1	4.5	6.6
	minimum value	5.8	8.4	10.8	2.2	5.3	4.2	3.0	3.1	4.7
	mean value	6.8 ± 1.2	9.0 ± 0.6	12.2 ± 1.2	3.2 ± 1.1	4.5 ± 0.8	4.4 ± 0.2	4.3 ± 1.1	4.0 ± 0.8	6.5 ± 2.6

3.6.2. Internal Bond Strength (IB)

The performance of chitosan as a binder in these new panels can be directly evaluated via the determination of the IB strength.

The average IB strength values of the prepared panels are presented in Figure 8. A statistical analysis of the IB strength results, including the median, minimum, maximum, mean and standard deviation values, is shown in Table 4.

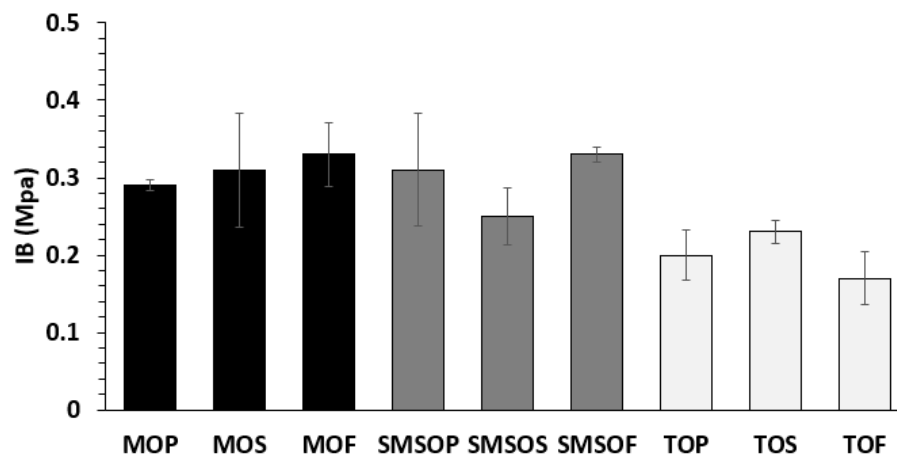


Figure 8. IB strength values of different panels.

Table 4. Statistical analysis of IB strength results for all formulations.

Formulations Labels	Mean Value (MPa)	Median Value (MPa)	Maximum Value (MPa)	Minimum Value (MPa)
MOP	0.29 ± 0.007	0.285	0.29	0.28
MOS	0.31 ± 0.074	0.32	0.39	0.22
MOF	0.33 ± 0.041	0.35	0.36	0.28
SMSOP	0.31 ± 0.073	0.3	0.39	0.25
SMSOS	0.25 ± 0.037	0.285	0.29	0.28
SMSOF	0.33 ± 0.009	0.335	0.34	0.33
TOP	0.20 ± 0.032	0.185	0.19	0.18
TOS	0.23 ± 0.015	0.23	0.24	0.22
TOF	0.17 ± 0.034	0.16	0.21	0.15

To satisfy the requirements of the relevant standard specifications EN 312, the IB strength value for wood particleboard intended to be used for general purposes in dry conditions must be above 0.28 MPa [42]. The IB values of the panels in this study varied from 0.17 to 0.33 MPa. M-based and SMS-based panels showed the highest IB (from 0.25 ± 0.037 to 0.33 ± 0.041 MPa), whereas T-based panels showed lower strength (between 0.17 ± 0.034 and 0.23 ± 0.015 MPa), which can be explained by the possible lower wettability of textile fibers by the chitosan binder. It can be pointed out that the use of oil-free pomace in MOF and SMSOF panels resulted in promising results, with improved IB values (0.33 ± 0.041 MPa) compared to panels containing OS or OP (0.25 ± 0.037 , 0.29 ± 0.007 and 0.31 ± 0.074 MPa). It is also clear that MOS showed the best IB properties between the OS-based panels. Its IB strength value (0.31 ± 0.074 MPa) was higher than that of SMSOS (0.25 ± 0.037 MPa) and of TOS (0.23 ± 0.015 MPa). All the M-based and SMS-based panels produced met the minimum requirements for the IB strength value of boards used for general purposes, according to EN 312. These results are competitive when compared to those obtained for wood fiber panels prepared at 190 °C using Organosolv thermostet lignin [43], comparable to those obtained for pure tannin and mixtures of glyoxalated lignin/tannin and tannins/synthetic resins [44], and comparable those of hazelnut husk boards bound with three different types of formaldehyde-based resins (urea-formaldehyde (UF), phenol formaldehyde (PF), melamine-formaldehyde (MUF)) [45]. All of these panels from the literature, in addition to our own produced panels, met the requirement set in the general-purpose product standards (EN 312), which shows that the chitosan used in this study is very useful, and can compete with traditional formaldehyde-based binders and other natural binders, such as tannin and lignin.

3.6.3. Compression

Figure 9 shows the compressive strengths of the various panels, which were in their native states before immersion as well as after immersion and drying. It should be noted that the highest compressive strength was achieved by OF-based panels compared to the

OP-based panels and OS-based ones. This shows that the use of oil-free pomace (without extractives) leads to a better mechanical behavior induced by better compaction and a better interface, as confirmed by microscopic observations (Figure 4). The same trend was already seen in the MOE results (Figure 7A). It can also be seen that the SMSOF panel achieved the highest compressive strength value (9.5 MPa), which is probably linked, in addition to the use of OF, to the presence of mycelium, which played the role of an additional intrinsic adhesive. On the other hand, after immersion in water for 5 days and drying, the compressive strength appears to have deteriorated for all panels. The OP-based panels maintained the best compressive strengths compared to the other WCP. These deteriorations in mechanical properties can be mainly associated with the fibers' decohesion, caused by the disappearance of the shiny layer of chitosan on the surface of the panels, which is clearly visible in Figure 10, indicating a partial dissolution of the binder. It can also be noted that pores and voids between reinforcements were created after immersion, showing interracial degradation. The same degradation of mechanical properties after immersion was also seen for pultruded kenaf fiber-reinforced composites after long-term immersion [46].

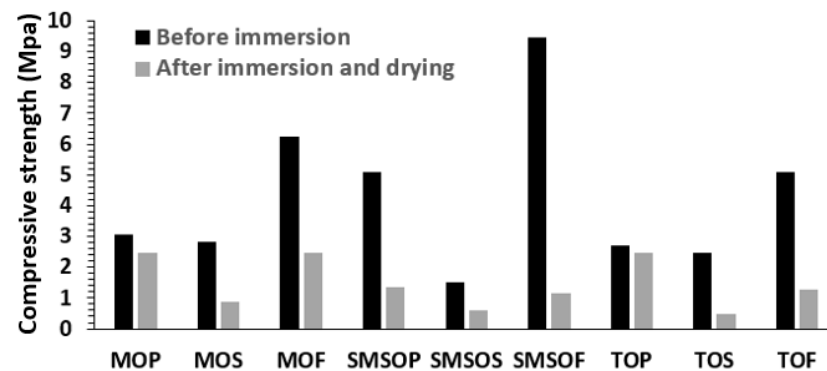


Figure 9. Compressive strength values (MPa) of the prepared WCP before and after the immersion test.

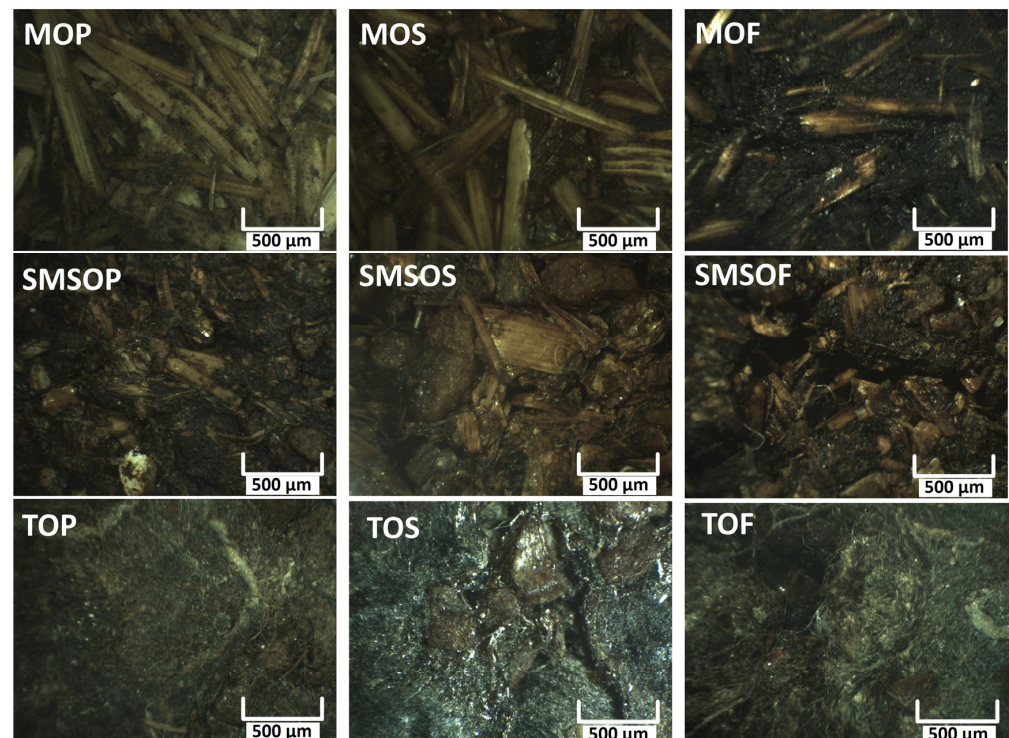


Figure 10. Microscopic observations of the surfaces of the different panels after immersion and drying, with a scale of 500 μm applied to all figures.

3.6.4. Critical Discussion of Data Using a Comparative Radar Chart

Figure 11 presents a radar chart analysis, which could offer critical insights into the comparative performances of the various material properties assessed in this study, with significant implications for their potential applications. In this chart, eight key parameters are encapsulated, including porosity (blue curve), bulk density (orange curve), internal bond (IB; dark green curve), thermal conductivity (light blue curve), dry (purple curve) and wet (light green curve) compressive strength, modulus of elasticity (MOE; dark blue curve), and modulus of rupture (MOR; brown curve), all of which have been normalized to a scale of 0 to 1, with each axis representing a different characteristic, to facilitate a direct comparison between the different formulations.

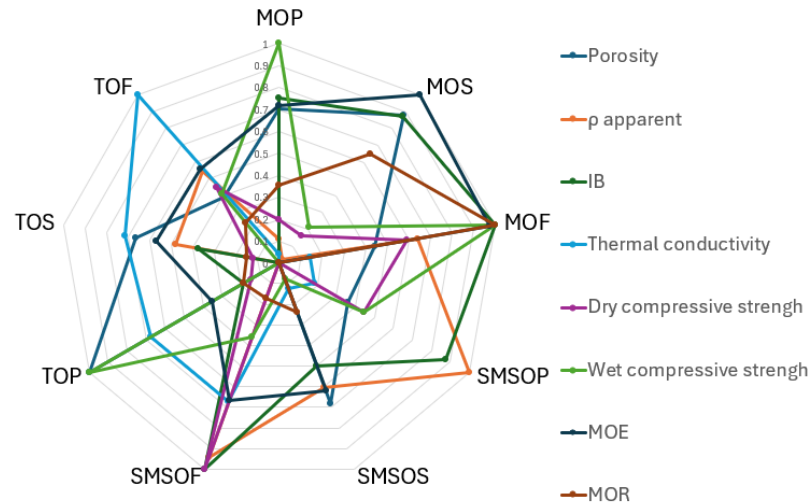


Figure 11. Global radar chart of normalized characterization values for various formulations.

In the radar chart results for porosity value, TOP shows the highest value among all samples, implying the freest and most openly structured sample. MOS and MOP closely follow. The other lower porosities are mainly related to panels containing oil-free pomace (TOF, MOF and SMSOF), indicating fewer visible pores and perhaps more compactness. Among all the formulations, SMSOF shows the lowest porosity; hence it is very dense. SMSOS and SMSOF have the highest apparent densities; this is in line with their low porosities. TOP, TOF and MOP have lower apparent densities because they have higher porosities. MOF and SMSOF depict higher internal bond strengths, as read on the radar chart for IB. This strong IB suggests that both formulations have excellent internal cohesion, making them ideal for use in applications where resistance to internal stresses is critical. SMSOS does not have a particularly high IB; instead, it has a lower value compared to MOF and SMSOF. This suggests that SMSOS might not be as strong in terms of internal cohesion, making it less suitable for applications where high internal bond strength is necessary. SMSOP shows a moderate IB value, which is better than that of SMSOS but not as high as those of MOF and SMSOF. This indicates that SMSOP has decent internal cohesion but might not be as robust as the top-performing formulations. MOP and MOS have the lowest IB values, indicating weaker internal cohesion. These materials may not withstand internal stresses as effectively as the other formulations, making them less suitable for structural applications where internal bond strength is important. Thermal conductivity is an essential factor in determining the insulation properties of the material. Based on the chart, the lowest thermal conductivity can be seen for SMSOF, which suggests it is the best insulator among the formulations. This property is ideal for applications where thermal insulation is crucial. Higher thermal conductivity is recorded for MOF and SMSOP, indicating they may not be as effective when used for insulation, but could be suitable for use in applications where moderate thermal transfer is acceptable. Compressive strength, both dry and wet, is a measure of the material's ability to withstand loads without failing. SMSOF and SMSOS exhibit the highest dry compressive strengths, making them ideal for

applications where load-bearing capacity is critical. MOP and MOS have the lowest dry compressive strengths, indicating they may be more prone to failure under dry conditions. SMSOP shows the highest wet compressive strength, indicating it retains its structural integrity even in moist conditions. This is important for applications where exposure to humidity or wet environments is expected. MOE is a measure of the material's stiffness, reflecting its ability to elastically deform under load. TOF and MOF have the highest MOE values, indicating they are the stiffest among the formulations, which is crucial for applications requiring minimal deformation under load. MOP and MOS show the lowest MOE values, suggesting they are less stiff and more prone to deformation. MOR is an indicator of the material's strength before failure. The chart shows that SMSOF and MOF exhibit the highest MOR values, suggesting they have the best load-bearing capacity before rupture. These materials are suitable for use in applications where high strength is required. MOS and MOP have the lowest MOR values, indicating they are less capable of withstanding high loads before breaking.

From the chart analysis, SMSOF and MOF emerge as the best-performing formulations overall. SMSOF excels in terms of properties such as low porosity, high internal bond strength, high density, and strong compressive strength, making it highly suitable for use in structural and insulation applications. MOF also performs well, with high internal bond strength, moderate porosity, and high modulus of rupture, making it versatile for a range of structural applications. On the other hand, MOP and MOS show worse performances across multiple properties, especially in terms of internal bond strength, modulus of elasticity, and compressive strength, suggesting they are less suitable for use in demanding structural applications, but may be used where lower weight and other properties are prioritized. SMSOS and SMSOP show mixed results, with strengths in specific areas like wet compressive strength and moderate internal bond strength. These formulations could be optimized further, depending on the specific application requirements.

In summary, SMSOF and MOF are recommended for use in applications requiring strong, cohesive, and insulating materials, while MOP and MOS are less suitable for high stress environments, but may serve in less demanding roles.

4. Conclusions

This study examined the production of novel eco-friendly chitosan-based composites for building applications using various agricultural wastes. The novelty of this study lies in the use of waste from the olive oil industry and mushroom cultivation as reinforcements in wood composite panels. A thorough analysis was conducted by preparing different panels using various parts of olive waste (olive pomace (OP), stones (OS), and oil-free pomace (OF)) combined with miscanthus, spent mushroom substrate, or recycled textile fibers. The prepared panels exhibit medium density, ranging between 685 and 907 kg/m³.

Notably, the incorporation of oil-free pomace in the panels led to very promising results, as the absence of extractives resulted in denser panels with fewer visible pores, thereby improving the rigidity, internal bonding strength, and compressive strength of the panels. Panels with hydrophobic superficial behavior were also produced due to the presence of residual fatty acids in the extractables. Additionally, the panels based on spent mushroom substrate achieved the highest densities (806–907 kg/m³) and the lowest porosity rates (3.4–15.8%) due to the softening and shrinkage of the present mycelium, while the panels based on miscanthus exhibited superior rigidity.

This study illustrates that low-value agricultural waste can be effectively utilized in promising applications in the composite panel sector, particularly for indoor use. Future research could focus on optimizing the mechanical properties and durability of these panels through advanced processing techniques, or by incorporating other sustainable additives. Moreover, exploring the scalability of this production process and assessing the environmental impact of these composites in real-world applications would be valuable. The results presented here have the potential to contribute significantly to the development of sustainable materials in the construction industry, offering eco-friendly alternatives for use as building materials that address both waste management and material innovation challenges.

Supplementary Materials: The following supporting information can be downloaded at: <https://www.mdpi.com/article/10.3390/appliedchem4030019/s1>, Figure S1: Force-displacement curve showing maximum force (Fmax), force levels (F1, F2), and corresponding displacements (a1, a2) during material deformation.

Author Contributions: Conceptualization, R.E.H., N.B. and Y.K.; methodology, Y.K., P.E.H., S.M. and N.B.; validation, R.E.H., J.D.M. and N.B.; investigation, Y.K., P.E.H., S.M. and R.E.H.; resources, R.E.H. and N.B.; writing—original draft preparation, Y.K., P.E.H., S.M. and R.E.H.; visualization, R.E.H., J.D.M., N.B., A.B. and P.L.; supervision, R.E.H., J.D.M. and N.B.; funding acquisition, R.E.H. and N.B. All authors have read and agreed to the published version of the manuscript.

Funding: This research was funded by the National Council for Scientific Research in Lebanon CNRS-L, Lebanese University (Lebanon) and Lorraine University (France): DrEAM Program.

Institutional Review Board Statement: Not applicable.

Informed Consent Statement: Not applicable.

Data Availability Statement: All data supporting the findings of this study are provided within the article and the Supplementary Materials.

Acknowledgments: Lorraine University is acknowledged for the support: DrEAM Entrant doctoral student mobility program. The authors gratefully acknowledge EARL GozennAr and Le Relais companies for freely supplying the reinforcement used in this study.

Conflicts of Interest: The authors declare no conflicts of interest.

References

1. Damette, O.; Delacote, P. Unsustainable Timber Harvesting, Deforestation and the Role of Certification. *Ecol. Econ.* **2011**, *70*, 1211–1219. [\[CrossRef\]](#)
2. Morillo, J.A.; Antizar-Ladislao, B.; Monteoliva-Sánchez, M.; Ramos-Cormenzana, A.; Russell, N.J. Bioremediation and Biovalorisation of Olive-Mill Wastes. *Appl. Microbiol. Biotechnol.* **2009**, *82*, 25–39. [\[CrossRef\]](#) [\[PubMed\]](#)
3. El Kassis, E.; Otazaghine, B.; El Hage, R.; Sonnier, R. Assessment of Olive Pomace Wastes as Flame Retardants. *J. Appl. Polym. Sci.* **2019**, *137*, 47715. [\[CrossRef\]](#)
4. Topal, H.; Atimtay, A.T.; Durmaz, A. Olive Cake Combustion in a Circulating Fluidized Bed. *Fuel* **2003**, *82*, 1049–1056. [\[CrossRef\]](#)
5. La Rubia-García, M.D.; Yebra-Rodríguez, Á.; Eliche-Quesada, D.; Corpas-Iglesias, F.A.; López-Galindo, A. Assessment of Olive Mill Solid Residue (Pomace) as an Additive in Lightweight Brick Production. *Constr. Build. Mater.* **2012**, *36*, 495–500. [\[CrossRef\]](#)
6. Aceña-Heras, S.; Novak, J.; Cayuela, M.L.; Peñalosa, J.M.; Moreno-Jiménez, E. Mushroom Cultivation in the Circular Economy. *Appl. Microbiol. Biotechnol.* **2018**, *102*, 7795–7803. [\[CrossRef\]](#)
7. Rezanian, S.; Hara, H. Environmentally Sustainable Applications of Agro-Based Spent Mushroom Substrate (SMS): An Overview Energy Generation and Wastewater Treatment Using Microalgae View Project Areas of Interest: English Language and Literature; Effects of Technology and Sociopsychological Aspects on Education and Instruction View Project Mohd Fadhil Md Din Universiti Teknologi Malaysia. *Artic. J. Mater. Cycles Waste Manag.* **2018**, *20*, 1383–1396. [\[CrossRef\]](#)
8. Cunha Zied, D.; Sánchez, J.E.; Noble, R.; Pardo-Giménez, A. Use of Spent Mushroom Substrate in New Mushroom Crops to Promote the Transition towards a Circular Economy. *Agronomy* **2020**, *10*, 1239. [\[CrossRef\]](#)
9. Rinker, D.L. Spent Mushroom Substrate Uses. In *Edible and Medicinal Mushrooms: Technology and Applications*; Wiley: Hoboken, NJ, USA, 2017; pp. 427–454. [\[CrossRef\]](#)
10. Phan, C.W.; Sabaratnam, V. Potential Uses of Spent Mushroom Substrate and Its Associated Lignocellulosic Enzymes. *Appl. Microbiol. Biotechnol.* **2012**, *96*, 863–873. [\[CrossRef\]](#)
11. Cunha Zied, D.; Pardo-Giménez, A. *Edible and Medicinal Mushrooms: Technology and Applications*; Wiley: Hoboken, NJ, USA, 2017.
12. Khoo, S.C.; Peng, W.X.; Yang, Y.; Ge, S.B.; Soon, C.F.; Ma, N.L.; Sonne, C. Development of Formaldehyde-Free Bio-Board Produced from Mushroom Mycelium and Substrate Waste. *J. Hazard. Mater.* **2020**, *400*, 123296. [\[CrossRef\]](#)
13. Xing, Y.; Brewer, M.; El-Gharabawy, H.; Griffith, G.; Jones, P. Growing and Testing Mycelium Bricks as Building Insulation Materials. *IOP Conf. Ser. Earth Environ. Sci.* **2018**, *121*, 022032. [\[CrossRef\]](#)
14. Jones, M.; Huynh, T.; Dekiwadia, C.; Daver, F.; John, S. Mycelium Composites: A Review of Engineering Characteristics and Growth Kinetics. *J. Bionanosci.* **2017**, *11*, 241–257. [\[CrossRef\]](#)
15. Eitzinger, J.; Kössler, C. Microclimatological Characteristics of a Miscanthus (*Miscanthus* Cv. Giganteus) Stand during Stable Conditions at Night in the Nonvegetative Winter Period. *Theor. Appl. Climatol.* **2002**, *72*, 245–257. [\[CrossRef\]](#)
16. El Bassam, N. *Energy Plant Species: Their Use and Impact on Environment and Development*; Routledge: London, UK, 2013; ISBN 1134255667.
17. Muthuraj, R.; Misra, M.; Mohanty, A.K. Injection Molded Sustainable Biocomposites from Poly(Butylene Succinate) Bioplastic and Perennial Grass. *ACS Sustain. Chem. Eng.* **2015**, *3*, 2767–2776. [\[CrossRef\]](#)
18. Eschenhagen, A.; Raj, M.; Rodrigo, N.; Zamora, A.; Labonne, L.; Evon, P.; Weleman, H. Investigation of Miscanthus and Sunflower Stalk Fiber-Reinforced Composites for Insulation Applications. *Adv. Civ. Eng.* **2019**, *2019*, 9328087. [\[CrossRef\]](#)

19. Muthuraj, R.; Misra, M.; Mohanty, A.K. Biodegradable Biocomposites from Poly(Butylene Adipate-Co-Terephthalate) and Miscanthus: Preparation, Compatibilization, and Performance Evaluation. *J. Appl. Polym. Sci.* **2017**, *134*, 45448. [[CrossRef](#)]
20. Khalaf, Y.; El Hage, P.; Dimitrova Mihajlova, J.; Bergeret, A.; Lacroix, P.; El Hage, R. Influence of Agricultural Fibers Size on Mechanical and Insulating Properties of Innovative Chitosan-Based Insulators. *Constr. Build. Mater.* **2021**, *287*, 123071. [[CrossRef](#)]
21. El Hage, R.; Khalaf, Y.; Lacoste, C.; Nakhil, M.; Lacroix, P.; Bergeret, A. A Flame Retarded Chitosan Binder for Insulating Miscanthus/Recycled Textile Fibers Reinforced Biocomposites. *J. Appl. Polym. Sci.* **2018**, *136*, 47306. [[CrossRef](#)]
22. Rubino, C.; Aracil, M.B.; Gisbert-Payá, J.; Liuzzi, S.; Stefanizzi, P.; Cantó, M.Z.; Martellotta, F. Composite Eco-Friendly Sound Absorbing Materials Made of Recycled Textile Waste and Biopolymers. *Materials* **2019**, *12*, 4020. [[CrossRef](#)]
23. Patti, A.; Cicala, G.; Acierno, D. Eco-Sustainability of the Textile Production: Waste Recovery and Current Recycling in the Composites World. *Polymers* **2020**, *13*, 134. [[CrossRef](#)]
24. El Hage, R.; Chrusciel, L.; Desharnais, L.; Brosse, N. Effect of Autohydrolysis of Miscanthus x Giganteus on Lignin Structure and Organosolv Delignification. *Bioresour. Technol.* **2010**, *101*, 9321–9329. [[CrossRef](#)] [[PubMed](#)]
25. Lacoste, C.; El, R.; Bergeret, A.; Corn, S.; Lacroix, P. Sodium Alginate Adhesives as Binders in Wood Fibers / Textile Waste Fibers Biocomposites for Building Insulation. *Carbohydr. Polym.* **2018**, *184*, 1–8. [[CrossRef](#)] [[PubMed](#)]
26. Mati-Baouche, N.; De Baynast, H.; Lebert, A.; Sun, S.; Lopez-Mingo, C.J.S.; Leclaire, P.; Michaud, P. Mechanical, Thermal and Acoustical Characterizations of an Insulating Bio-Based Composite Made from Sunflower Stalks Particles and Chitosan. *Ind. Crops Prod.* **2014**, *58*, 244–250. [[CrossRef](#)]
27. Dutta, P.K.; Joydeep, D.; Tripathi, V.S. Chitin and Chitosan: Properties and Applications. *J. Sci. Ind. Res.* **2004**, *63*, 20–31. [[CrossRef](#)]
28. Barbosa, M.A.; Granja, P.L.; Barrias, C.C.; Amaral, I.F. Polysaccharides as Scaffolds for Bone Regeneration. *Itbm-Rbm* **2005**, *26*, 212–217. [[CrossRef](#)]
29. Hemmilä, V.; Adamopoulos, S.; Karlsson, O.; Kumar, A. Development of Sustainable Bio-Adhesives for Engineered Wood Panels—A Review. *RSC Adv.* **2017**, *7*, 38604–38630. [[CrossRef](#)]
30. Antov, P.; Savov, V.; Neykov, N. Sustainable Bio-Based Adhesives for Eco-Friendly Wood Composites a Review. *Wood Res.* **2020**, *65*, 51–62. [[CrossRef](#)]
31. Pizzi, A. Wood Products and Green Chemistry. *Ann. For. Sci.* **2016**, *73*, 185–203. [[CrossRef](#)]
32. Sørensen, A.; Teller, P.J.; Hilstrøm, T.; Ahring, B.K. Hydrolysis of Miscanthus for Bioethanol Production Using Dilute Acid Pre-soaking Combined with Wet Explosion Pre-Treatment and Enzymatic Treatment. *Bioresour. Technol.* **2008**, *99*, 6602–6607. [[CrossRef](#)]
33. Medouni-haroune, L.; Zaidi, F.; Medouni-adrar, S.; Kecha, M. Olive Pomace: From an Olive Mill Waste to a Resource, an Overview of the New Treatments. *J. Crit. Rev.* **2018**, *5*, 1–6. [[CrossRef](#)]
34. Khedari, J.; Suttisonk, B.; Pratinthong, N.; Hirunlabh, J. New Lightweight Composite Construction Materials with Low Thermal Conductivity. *Cem. Concr. Compos.* **2001**, *23*, 65–70. [[CrossRef](#)]
35. Yenier, Z.; Seki, Y.; Şen, I.; Sever, K.; Mermer, Ö.; Sarikanat, M. Manufacturing and Mechanical, Thermal and Electrical Characterization of Graphene Loaded Chitosan Composites. *Compos. Part B Eng.* **2016**, *98*, 281–287. [[CrossRef](#)]
36. Huhtamäki, T.; Tian, X.; Korhonen, J.T.; Ras, R.H.A. Surface-Wetting Characterization Using Contact-Angle Measurements. *Nat. Protoc.* **2018**, *13*, 1521–1538. [[CrossRef](#)] [[PubMed](#)]
37. Oliveira, S.L.; Mendes, R.F.; Mendes, L.M.; Freire, T.P. Particleboard Panels Made from Sugarcane Bagasse: Characterization for Use in the Furniture Industry. *Mater. Res.* **2016**, *19*, 914–922. [[CrossRef](#)]
38. Bektas, I.; Guler, C.; Kalaycioglu, H.; Mengeloglu, F.; Nacar, M. The Manufacture of Particleboards Using Sunflower Stalks (*Helianthus annuus* L.) and Poplar Wood (*Populus alba* L.). *J. Compos. Mater.* **2005**, *39*, 467–473. [[CrossRef](#)]
39. Yang, H.-S.; Kim, D.-J.; Kim, H.-J. Rice Straw–Wood Particle Composite for Sound Absorbing Wooden Construction Materials. *Bioresour. Technol.* **2003**, *86*, 117–121. [[CrossRef](#)]
40. Nemli, G.; Kırıcı, H.; Serdar, B.; Ay, N. Suitability of Kiwi (*Actinidia sinensis* Planch.) Prunings for Particleboard Manufacturing. *Ind. Crops Prod.* **2003**, *17*, 39–46. [[CrossRef](#)]
41. Guler, C.; Copur, Y.; Tascioglu, C. The Manufacture of Particleboards Using Mixture of Peanut Hull (*Arachis hypogaea* L.) and European Black Pine (*Pinus nigra* Arnold) Wood Chips. *Bioresour. Technol.* **2008**, *99*, 2893–2897. [[CrossRef](#)]
42. EN 312; Particleboards: Specifications. British Standard Institution: London, UK, 2010.
43. El Hage, R.; Brosse, N.; Navarrete, P.; Pizzi, A. Extraction, Characterization and Utilization of Organosolv Miscanthus Lignin for the Conception of Environmentally Friendly Mixed Tannin/Lignin Wood Resins. *J. Adhes. Sci. Technol.* **2012**, *25*, 1549–1560. [[CrossRef](#)]
44. Ping, L.; Hage, R.E.L.; Pizzi, A.; Guo, Z.D.; Brosse, N. Extraction of Polyphenolics from Lignocellulosic Materials and Agricultural Byproducts for the Formulation of Resin for Wood Adhesives. *J. Biobased Mater. Bioenergy* **2012**, *5*, 460–465. [[CrossRef](#)]
45. Çöpür, Y.; Güler, C.; Akgül, M.; Taşçıoğlu, C. Some Chemical Properties of Hazelnut Husk and Its Suitability for Particleboard Production. *Build. Environ.* **2007**, *42*, 2568–2572. [[CrossRef](#)]
46. Mazuki, A.A.M.; Akil, H.M.; Safiee, S.; Ishak, Z.A.M.; Bakar, A.A. Degradation of Dynamic Mechanical Properties of Pultruded Kenaf Fiber Reinforced Composites after Immersion in Various Solutions. *Compos. Part B Eng.* **2011**, *42*, 71–76. [[CrossRef](#)]

Disclaimer/Publisher's Note: The statements, opinions and data contained in all publications are solely those of the individual author(s) and contributor(s) and not of MDPI and/or the editor(s). MDPI and/or the editor(s) disclaim responsibility for any injury to people or property resulting from any ideas, methods, instructions or products referred to in the content.